D0 Note 6473-CONF

FERMILAB-CONF-16-383-PPD, Cavendish-HEP-16/15, TTK-16-36

Measurement of the pole mass of the top quark using differential $t\bar{t}$ cross sections in $p\bar{p}$ collisions at $\sqrt{s} = 1.96$ TeV

The D0 collaboration,
and M.Czakon (RWTH Aachen), P.Fiedler (RWTH Aachen),
D.Heymes (U of Cambridge), and A.Mitov (U of Cambridge)

(Dated: September 20, 2016)

The differential $t\bar{t}$ cross sections, measured as a function of the transverse momentum of the top quark and the invariant mass of the $t\bar{t}$ system, are employed to determine the pole mass of the top quark. The data corresponds to an integrated luminosity of 9.7 fb^{-1}, collected with the D0 detector of the Fermilab Tevatron. Precise calculations at next-to-next-to leading order in perturbative quantum chromodynamics provide the absolute differential cross sections that are employed to extract the pole mass of the top quark.We measure the pole mass of the top quark to be $169.1 \pm 2.5\,(\text{tot.})$ GeV.

I. INTRODUCTION

The top quark is the heaviest known elementary particle [1, 2] and the discovery of the Higgs boson [3, 4] marks the completion of the very successful standard model (SM). However, the top quark mass (m_t) in the SM is a completely free parameter and thus we rely on measurements. The most precise measurements of m_t with a precision better than 0.5% use 'direct techniques' [5, 6], for example mass reconstruction relying on the top quark decay particles or matrix element techniques. The world average of these direct measurements currently is $m_t = 173.34 \pm 0.76$ GeV [7], while the latest Tevatron combination including updated direct measurements is 174.30 ± 0.65 GeV [8]. The direct measurements are based on analysis techniques relying on $t\bar{t}$ events from Monte Carlo (MC) simulation for several values of the top quark mass. Applying these techniques to data provides a mass corresponding to the scheme used for the top quark mass implemented in the MC that we refer to as the "MC mass" or m_t^{MC}. Theoretical arguments suggest that m_t^{MC} as measured by the direct mass measurements is within about 1 GeV of the well-defined pole mass m_t^{pole} [9]. A calibration of the relationship between m_t^{MC} in PYTHIA8 [10] and m_t^{pole} has recently been done in Ref. [11] by comparing theoretical calculations for $e^+e^- \to t\bar{t}$.

An alternate approach where m_t^{pole} is extracted from the total $t\bar{t}$ cross section, not subject to this theoretical uncertainty, has been taken by the ATLAS, CMS and D0 collaborations [12–15]. The most recent m_t^{pole} extraction by D0 [15] uses the inclusive $t\bar{t}$ cross section $\sigma(t\bar{t})$.

In this note we use a novel technique based on extracting the theoretically well-defined m_t^{pole} from a comparison of differential $t\bar{t}$ cross sections predicted by perturbative QCD (pQCD) at next-to-leading order (NLO) and at next-to-next-to leading order (NNLO) with the measured differential distributions. We use the results from the dependence of the differential cross section on the invariant mass of the top and anti-top quark pair, $m(t\bar{t})$, and on the transverse momentum of the top and anti-top quarks (p_T^{top}) in the D0 Run II data sample [16]. The index "top" in p_T^{top} refers to either t or $\bar{t}$ quarks. The $\not\!\!E_T$ provides the initial estimate for the p_T of the neutrino. The longitudinal momentum $p_z(\nu)$ is estimated by constraining the mass of the W boson decay products to 80.4 GeV. Together with all possible jet-quark assignments there is 24 possible solutions for reconstructing the $t\bar{t}$ decay topology. We use a kinematic reconstruction method that seeks the best match to the top quark topology as determined by lowest χ^2. This reconstruction method is applied in the same way to data and MC, more details on the reconstruction method are given in Ref. [16].

This document was prepared by [D0 Collaboration] using the resources of the Fermi National Accelerator Laboratory (Fermilab), a U.S. Department of Energy, Office of Science, HEP User Facility. Fermilab is managed by Fermi Research Alliance, LLC (FRA), acting under Contract No. DE-AC02-07CH11359.

II. QCD CALCULATIONS

We follow Ref. [17] to obtain the absolutely normalized $m(t\bar{t})$ and $p_T^{\rm top}$ cross section distributions for the following set of top quark masses: $m_t^{\rm pole} = 155, 160, 165, 170, 173.3, 175, 180, 185, 190$ GeV. The calculation for $m_t^{\rm pole} = 173.3$

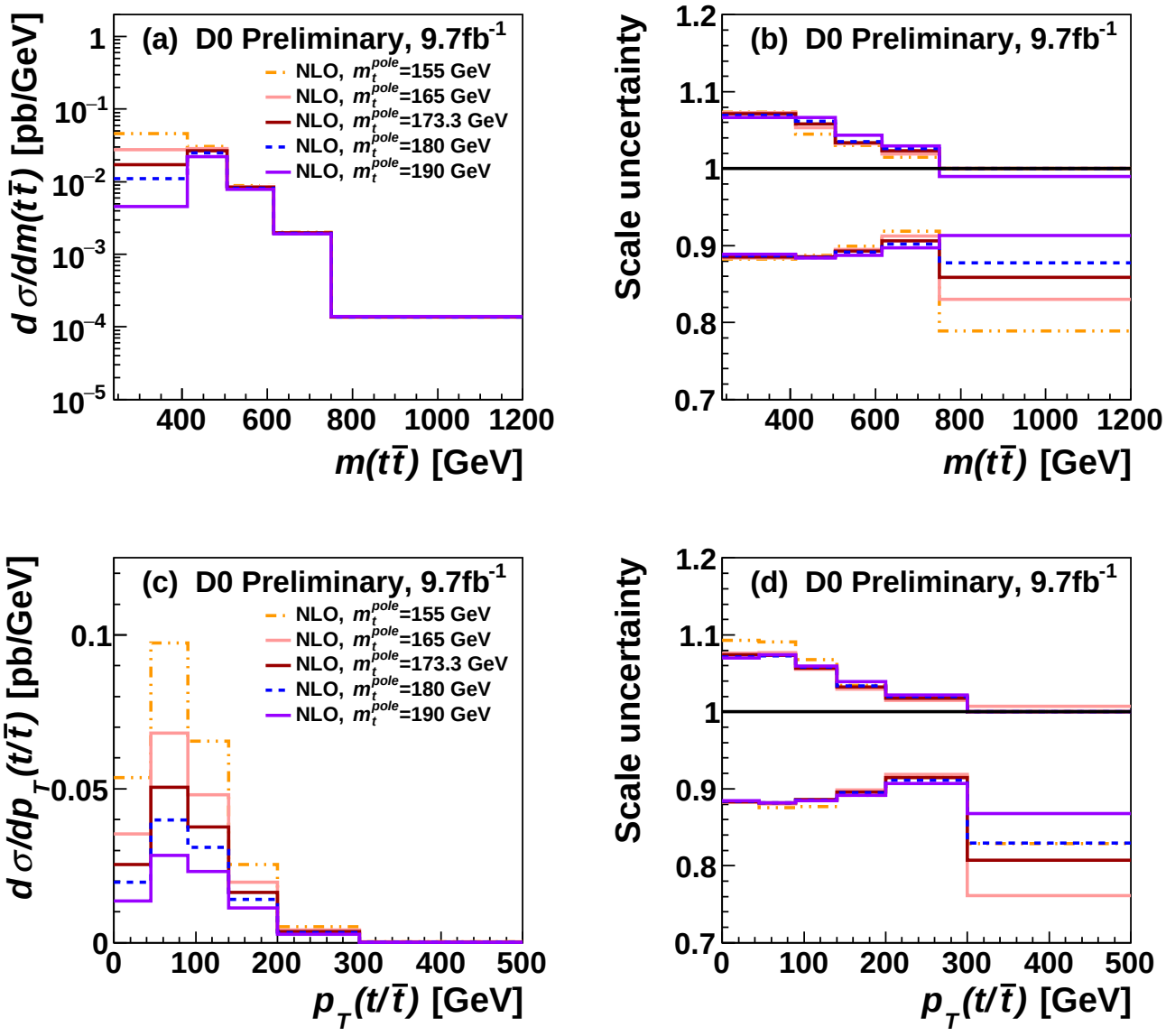

FIG. 1. The different calculations at NLO (MSTW2008 PDF) for five selected values of the top quark mass for (a) $m(t\bar{t})$ and (c) $p_T^{\rm top}$. A ratio of the calculated cross section using independent μ_R and μ_F changes by a factor of 2 relative to the calculated cross section using the default scale choice is shown in (b) for $m(t\bar{t})$ and in (d) for $p_T^{\rm top}$. The horizontal solid line at 1 indicates the nominal scale choice for any $m_t^{\rm pole}$.

GeV coincides with the one in Ref. [17] and the results for the other masses are new. The calculations use the same bins as the original differential measurements from D0 [16]. The differential distributions are computed at NLO and NNLO pQCD, but they do not include soft-gluon resummations or any other partial corrections beyond NNLO. We have checked that the sum over all bins, including overflow events, agrees with the calculated total cross section at NNLO pQCD [18–21] produced with the `Top++` program [22] using the same parameters. Nevertheless, these fixed-order distributions provide an inclusive cross-section that is lower than the NNLO+NNLL resummed cross section [23] generated using the default `Top++` program by about 2%.

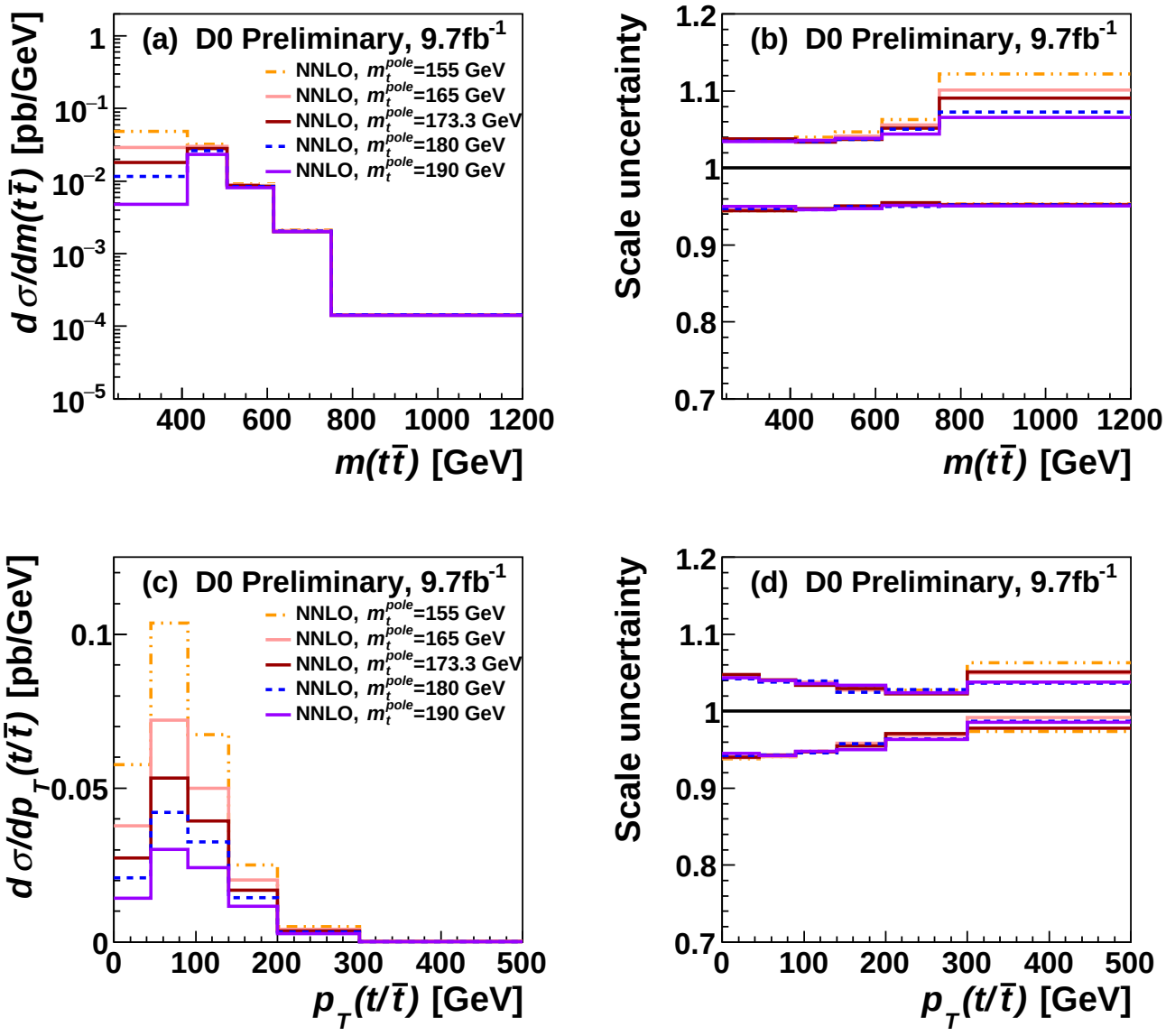

FIG. 2. The different calculations at NNLO (MSTW2008 PDF) for five selected values of the top quark mass for (a) $m(t\bar{t})$ and (c) $p_T^{\rm top}$. A ratio of the calculated cross section using independent μ_R and μ_F changes by a factor of 2 relative to the calculated cross section using the default scale choice is shown in (b) for $m(t\bar{t})$ and in (d) for $p_T^{\rm top}$. The horizontal solid line at 1 indicates the nominal scale choice for any $m_t^{\rm pole}$.

The calculation is performed for four parton-density distribution functions (PDF) at either NLO or NNLO: 'MSTW2008(n)nlo68cl' (MSTW2008) [24], 'CT10(n)nlo' (CT10) [25], 'NNPDF23_(n)nlo_FFN_NF5_as_0118' (NNPDF23) [26], and 'HERAPDF15(N)NLO_EIG' (HERAPDF15) [27]. We refer to the PDFs from MSTW, CT and NNPDF as global PDFs since they include all available experimental data, while HERAPDF is following a different approach using only the unique *ep* data for their PDF fit. We follow the PDF4LHC approach for determining a PDF uncertainty based on the three global PDF sets [28]. The value of α_S is obtained from the LHAPDF interface [29]. This approach ensures consistency between the value of α_S used in the partonic calculation and in the parton distributions. Electroweak corrections are likely too small to be relevant in the present study and are not included. Finally, uncertainties in the MC integration are small, typically within 1% in each bin (see Ref. [17] for more details). The calculations use fixed non-dynamic renormalization and factorization scales (μ_R and μ_F), both chosen to be equal to m_t. Scale uncertainties are obtained through independent changes of μ_R and μ_F around their central values by a factor of two:

$0.5 \leq \mu_F/\mu_R \leq 2$ [30] with the envelope of these variations assigned as scale uncertainties. We do not compute the uncertainties associated with each choice of PDF since these are generally smaller than the uncertainty from varying μ_R and μ_F independently in pQCD [17] and thus when added in quadrature contribute little to the total theoretical uncertainties. An alternative way of judging the PDF dependence is through a comparison of $m_t^{\rm pole}$ extractions based on different PDF sets as provided below.

The theoretical inclusive $t\bar{t}$ cross section is defined through the addition of the bins in the calculation for a particular top quark mass. Compared to NNLO, the NLO differential calculation provides a lower cross section for all masses, and this is reflected in a smaller value of $m_t^{\rm pole}$ for the NLO calculation.

Figure 1 shows the differential cross sections for five different m_t values calculated at NLO as a function of $m(t\bar{t})$ and $p_T^{\rm top}$, and provides ratios of the up and down changes of μ_R and μ_F for a particular $m_t^{\rm pole}$ to the corresponding calculation using the default scale choice. The bins for the largest values in both the $m(t\bar{t})$ and $p_T^{\rm top}$ distributions do not contain overflow events. The scale uncertainties are $\approx 5\%$, except at larger values of $m(t\bar{t})$ and $p_T^{\rm top}$ where they are up to 20%.
Figure 2 shows the same collection of cross section distributions, but calculated at NNLO QCD. As expected scale uncertainties are smaller with values of at most 5% for $p_T^{\rm top}$, whereas at highest $m(t\bar{t})$, values of 10% are observed.

III. SUMMARY OF DIFFERENTIAL CROSS SECTION MEASUREMENT

The proper extraction of $m_t^{\rm pole}$ from differential cross sections, corrected for detector effects by using matrix unfolding, relies on the use of a covariance matrix. Since the results from Ref. [16] rely on matrix unfolding we briefly discuss the method in the following.

A. Unfolding the differential cross section

For a quantity X_i, where i denotes an individual bin, the differential cross section is measured as:

$$\frac{d\sigma}{dX_i} = \frac{N_i^{\rm sig}}{\epsilon \cdot \mathcal{L} \cdot \mathcal{B} \cdot \Delta X_i} \ , \tag{1}$$

where $N_i^{\rm sig}$ is the number of background-subtracted signal events obtained using an unfolding procedure defined later in this section, ϵ is the detector efficiency times acceptance, $\mathcal{L}$ is the integrated luminosity, $\mathcal{B}$ is the branching ratio for the final state being considered, and ΔX_i is the bin width. For $t\bar{t}$ ℓ+jets events we use $\mathcal{B}(t\bar{t} \to e + \text{jets}) = 0.171$ and $\mathcal{B}(t\bar{t} \to \mu + \text{jets}) = 0.172$, both with uncertainties of 0.8% [32]. These values include electrons and muons stemming from the leptonic decay of τ leptons ($\tau_\ell \to \ell\nu_\ell\nu_\tau$).

Data are corrected for detector effects such as migrations, efficiencies, and acceptance by means of a regularized matrix-unfolding method [33–36] to the parton level in the full phase space. A regularization is needed to invert the matrix and to prevent numerical instabilities in the matrix inversion. The response matrix $\mathbf{A}$, which reflects the efficiency and the resolution of the D0 detector, relates the distributions in a reconstructed variable ($\mathbf{y}_{rec}$) to distributions of a variable at the unfolded or generator level ($\mathbf{x}_{true}$):

$$\mathbf{A} \cdot \mathbf{x}_{true} = \mathbf{y}_{rec} \ . \tag{2}$$

Each matrix element A_{ij} gives the probability for an event originating in bin j of $\mathbf{x}_{true}$ to be measured in bin i of $\mathbf{y}_{rec}$. The response matrix is determined from simulation, and has twice as many bins at the reconstruction level as at the generator level to provide detailed information on the probability distribution and to improve thereby the accuracy of the unfolding procedure [35]. The unfolding reduces the influence of model assumptions in determining the cross sections relative to just a bin-by-bin correction.

Regularized unfolding [37] is based on a χ^2 minimization using a migration matrix $\mathbf{A}$ extracted from fully simulated MC events, as implemented in the TUnfold package [36]:

$$\chi^2 = \sum_i \frac{\left(y_i^{\rm data} - \sum_j A_{ij} \cdot x_j^{\rm true}\right)^2}{\left(\delta y_i^{\rm data}\right)^2} + \sum_{ij} \tau^2 \times L_{ij}(L_{ij})^T \tag{3}$$

where the input to the χ^2 minimization reflects the data vector $y_i^{\rm data}$ with corresponding uncertainties $\delta y_i^{\rm data}$. The true unfolded vector is given by $x_j^{\rm true}$. The regularization strength τ and matrix condition $\mathbf{L}$ represent a penalty for any large local fluctuations that occur when the matrix is inverted. This procedure reduces the statistical correlations among neighboring bins introduced through the matrix unfolding. There are several ways to implement the penalty [36], e.g. through single bins that can be regularized based on their size, or neighboring bins can be taken into account using criteria such as the first or second derivative function. For the measurement used to extract $m_t^{\rm pole}$, we employ a first derivative criterion in which case $\mathbf{L}$ is initialized to $L_{i,i} = -1$ and $L_{i,i+1} = +1$ while all other entries are zero [36].

The covariance matrix is given by

$$\mathbf{V_{xx}} = \mathbf{B V_{yy} B}^T, \text{ where } \mathbf{B} = \mathbf{E A}^T {\mathbf{V_{yy}}}^{-1}, \ \mathbf{E} = \left(\mathbf{A}^T {\mathbf{V_{yy}}}^{-1} \mathbf{A} + \tau^2 \mathbf{L}^T \mathbf{L}\right)^{-1} \tag{4}$$

where $\mathbf{V_{yy}}$ is a diagonal matrix containing the squares of the uncertainties of the measurement. The statistical uncertainties for the unfolded result are given by the diagonal elements of $\mathbf{V_{xx}}$. However, to make full use of the unfolded cross sections, the full covariance matrix is needed. The unfolded vector $\mathbf{x}$ is given by:

$$\mathbf{x}^{\rm true} = \mathbf{A}^T {\mathbf{V_{yy}}}^{-1} \mathbf{A} \left(\mathbf{A}^T \cdot {\mathbf{V_{yy}}}^{-1} \cdot \mathbf{y}^{\rm data} + \tau^2 \cdot \mathbf{L}^T \mathbf{L} \cdot \mathbf{x_0}\right) \tag{5}$$

where x_0 is an initial distribution taken from the generated quantities of the migration matrix. We use the full covariance matrix, as provided by the algorithm to calculate the χ^2 between an unfolded differential data cross section and a calculated cross section for a particular value of $m_t^{\rm pole}$.

Since D0 published the differential cross sections [16] D0 also made a new measurement of the total $\sigma(t\bar{t})$ [15]. That measurement of the inclusive $t\bar{t}$ cross section employs a reduced uncertainty in luminosity of 4.3% compared to 6.1% in the measurement of differential cross sections [16]. The selection of $t\bar{t}$ events in the two measurements is very similar with respect to effects that affect the luminosity measurement. Hence, we can transfer the reduced uncertainty in luminosity to the already measured differential cross sections. The uncertainty in luminosity is part of the published covariance matrices of the differential cross sections, but it was added assuming 100% correlation, which allows for an adjustment of the uncertainty in luminosity. Following the adjustment we consistently re-invert the covariance matrix for the extraction of $m_t^{\rm pole}$.

B. Experimental systematic uncertainties

Table I summarizes the experimental systematic uncertainties and their impact on the differential cross sections. More details can be found in Ref. [16].

The uncertainties in modeling the $t\bar{t}$ signal include effects related to alternative signal generator, top quark mass and kinematics as well as to the background subtraction method. Hadronization effects are estimated by comparing MC@NLO +HERWIG [38, 39] to ALPGEN +PYTHIA [40, 41] for the signal. This represents a large variation, which includes differences in acceptance that are larger compared to differences from ALPGEN +PYTHIA for a different top quark mass. Another part of the signal model uncertainty arises from using a different top quark mass during the unfolding process, where we employ two MC samples with $m_t = 175$ GeV and $m_t = 170$ GeV and scale the resulting difference to a top mass uncertainty of 0.9 GeV matching the uncertainty of the Tevatron combination at the time the differential cross sections were published. The transverse momentum of the $t\bar{t}$ pair is not very well modeled by MC [42], and we assign the full difference between data and MC as part of the signal model uncertainty. Differences in the W+jets distributions from uncertainty in the choice of the PDF are small in regions of good statistical precision, whereas at higher $m(t\bar{t})$ or $p_T^{\rm top}$, differences are about 30−40%, which affects the background-subtracted distributions prior to the unfolding. However, W+jets contribute only 12−15% to the sample composition, and the impact of this background related signal uncertainty is therefore small but nonetheless included.

Uncertainties on detector modeling include effects due to trigger efficiency as well as object reconstruction that includes the lepton reconstruction and identification efficiency [43, 44], as well as effects due to the jet energy scale, jet resolution and jet identification [45]. Furthermore, we account for the difference in jet response between MC events and data, which changes with jet kinematics and depends on the flavor of the parton that initiates the jet [45]. We rely on the identification of b jets, and include the related systematic uncertainties on b-, c- and light-quark identification, as well as b-fragmentation [46]. A 4.3% uncertainty in luminosity is assigned to the unfolded data.

Uncertainties on the modeling of the background account for effects from the normalization of W+jets events, the uncertainties on the misidentified and true lepton selection rates, as well as uncertainties on the predicted cross sections for diboson and single top quark processes.

Experimental systematic uncertainties on the measurement technique include the procedural uncertainty of the chosen matrix unfolding method, and effects due to limited number of MC events.

Systematic error source	$\delta^{\rm up}_{\rm incl,rel}$ [%]	$\delta^{\rm down}_{\rm incl,rel}$ [%]	Range of uncertainty [%]
Signal model:			
Alternative signal model	+5.17	−4.28	1 − 10
t-quark mass dependence	+0.32	−0.35	1 − 3
$p_T^{t\bar{t}}$ missmodeling	+0.79	−0.67	1 − 4
PDF (CTEQ6M 40 error sets)	−2.96	+3.38	1 − 4
Detector model:			
Trigger efficiency	+2.50	−2.50	2.5 − 2.5
Lepton ID	+0.51	−0.53	1 − 3
Jet energy scale	+2.41	−2.50	1 − 20
Jet energy resolution	+0.37	−0.38	1 − 2
Jet Identification	+0.31	−0.31	1 − 2
Jet response correction	−0.91	+0.76	1 − 6
b-tagging Uncertainty	+1.57	−1.58	1 − 3
b-fragmentation	+0.09	−0.09	1 − 1
Vertex confirmation	−0.82	+0.84	1 − 1
Luminosity*	+4.30	−4.30	4.3 − 4.3
Background model:			
W+jets heavy flavor scale factor	+0.75	−0.78	2 − 8
True and Fake lepton efficiencies	+0.55	−0.57	1 − 2
Theoretical cross section prediction	+1.58	−1.47	1 − 3
Measurement technique:			
Procedural (Unfolding)	+0.18	−0.18	1 − 2
Total systematic uncertainty	+8.65	−8.28	
Total statistical uncertainty	+7.50	−7.50	

TABLE I. Table of systematic uncertainties on the differential cross sections for uncorrelated systematic sources are given as inclusive values combining all bins, and as range of uncertainty indicating the minimum and maximum uncertainty across all bins of the distributions. Values are as published in Ref. [16] with the exception of the luminosity uncertainty.

IV. DIFFERENTIAL CROSS SECTIONS

Figures 3 and 4 show the measured differential cross sections $m(t\bar{t})$ and $p_T^{\rm top}$ together with calculated cross sections for a series of different values of $m_t^{\rm pole}$, as well as the ratio of theoretical to measured values. We show the representative case using the MSTW2008 PDF; other PDF choices show a similar behavior as discussed in the next Section. Figure 3(a) shows the unfolded distribution for $m(t\bar{t})$ at the parton level for data compared to the theoretical calculations for selected values of input $m_t^{\rm pole}$. The ratios of the calculations to data are shown in (b), highlighting the sensitivity to the top quark mass in the threshold region. Figure 4 shows the same comparison for the $p_T^{\rm top}$ distributions, indicating improved sensitivity to $m_t^{\rm pole}$ relative to the $m(t\bar{t})$ variable.

V. DETERMINATION OF THE POLE MASS

We form a χ^2 that compares the measured differential cross sections with the theoretical calculation at the parton level. The χ^2 is defined by:

$$\chi^2 = \sum_{i,j} (x_i^{\rm true} - x_i^{\rm theo}) \cdot \mathbf{V}^{-1}_{\mathbf{xx;\ ij}} \cdot (x_j^{\rm true} - x_j^{\rm theo}), \tag{6}$$

where i and j are bin indices in either the $m(t\bar{t})$ or the $p_T^{\rm top}$ cross sections. We use the measured differential cross sections [16] for the extraction of $m_t^{\rm pole}$, after re-deriving the covariance matrix to account for the reduction relative to Ref. [16] in the uncertainty in integrated luminosity. The full covariance matrix (see Eqn. 4) is then inverted and employed to calculate the χ^2, thereby providing the correlations among the bins in the measured spectra, as well as the statistical and systematic uncertainties in the data. We extract $m_t^{\rm pole}$ for the four PDF sets and, using results from the three global PDF sets, provide an average value of $m_t^{\rm pole}$ with an additional theoretical uncertainty based on their spread.

We perform a parabolic fit, as shown in Figures 5 to 7, to the χ^2 distributions using the cross sections in $m(t\bar{t})$, $p_T^{\rm top}$

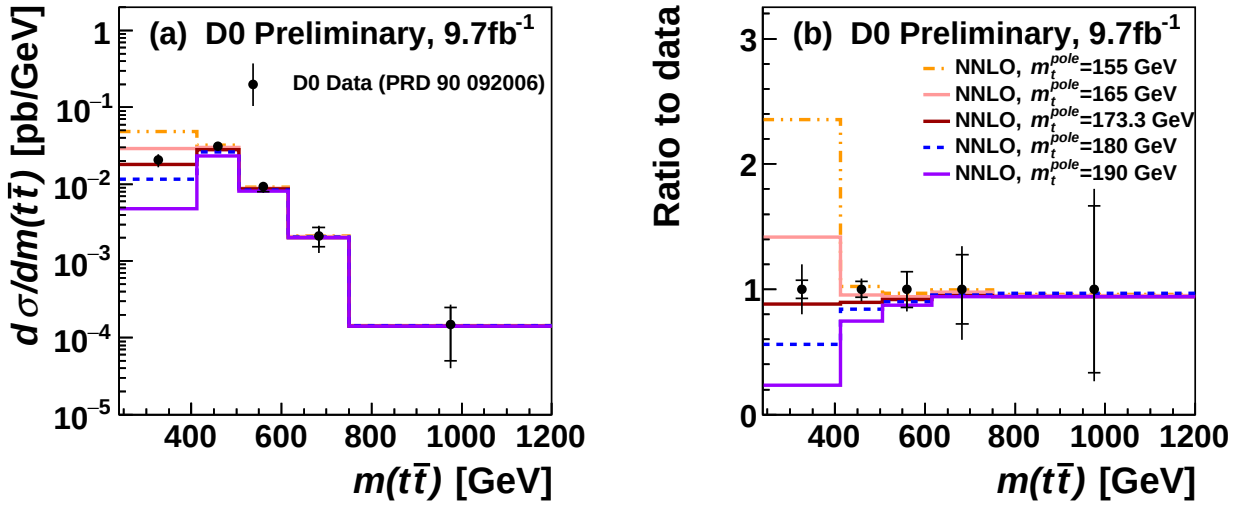

FIG. 3. Unfolded $m(t\bar{t})$ distribution in data (a) compared to theoretical calculations at NNLO pQCD for selected input values of $m_t^{\rm pole}$, and (b) the calculated distributions divided by the data. The inner error bars correspond to the statistical uncertainties and the outer error bars to the total uncertainties.

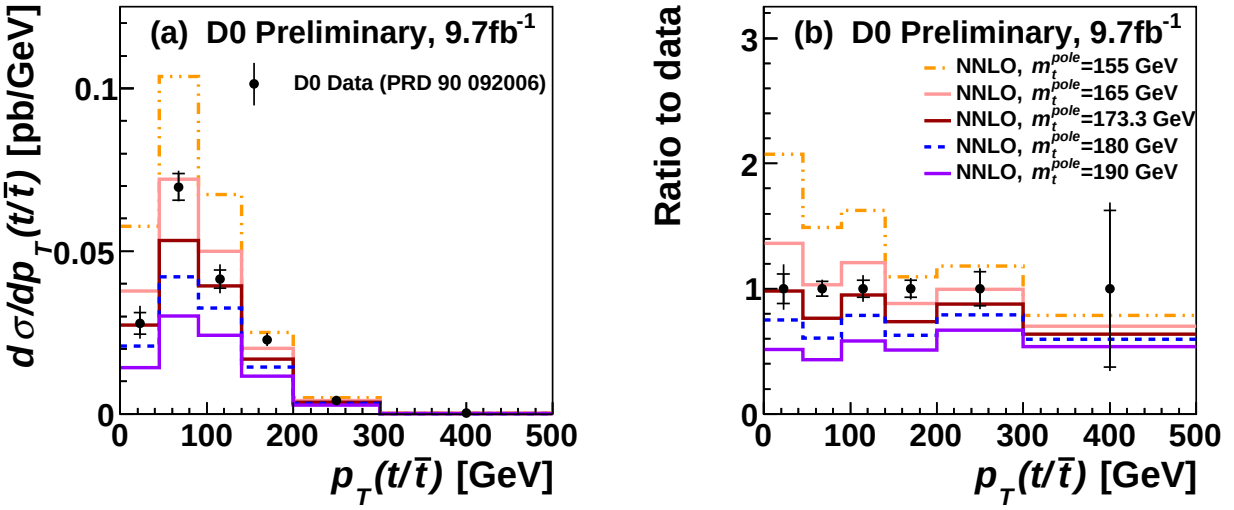

FIG. 4. Unfolded $p_T^{\rm top}$ distribution in data (a) compared to theoretical calculations at NNLO pQCD for selected input values of $m_t^{\rm pole}$, and (b) the calculated distributions divided by the data. The inner error bars correspond to the statistical uncertainties and the outer error bars to the total uncertainties.

or their combination, to determine the minimum of the χ^2, which represents $m_t^{\rm pole}$. The fit is limited to 160 – 180 GeV, which is the part of the distribution that best follows a parabolic shape. The number of degrees of freedom (n.d.f.) is six. The combined experimental and theoretical uncertainty on the extracted $m_t^{\rm pole}$ is defined using the criterion that $\Delta\chi^2 = 1$ relative to the minimum of the fitted parabola.

For each trial top quark mass we use the NLO and NNLO calculations (with the appropriate associated PDFs) to form a χ^2 according to Eqn. 6. Table II shows the $m_t^{\rm pole}$ results for all four PDF sets considered at either NLO

or NNLO. Figure 5 shows, for the MSTW2008 PDF as an example, the χ^2 distribution for the comparisons of data and theory at (a) NLO and at (b) NNLO as a function of $m_t^{\rm pole}$. The shaded bands indicate the uncertainties in the calculated values as the renormalization and factorization scales are varied. The solid line indicates the 2$^{\rm nd}$ order polynomial used to extract the minimum, which represents the value of $m_t^{\rm pole}$. The corresponding χ^2 distributions

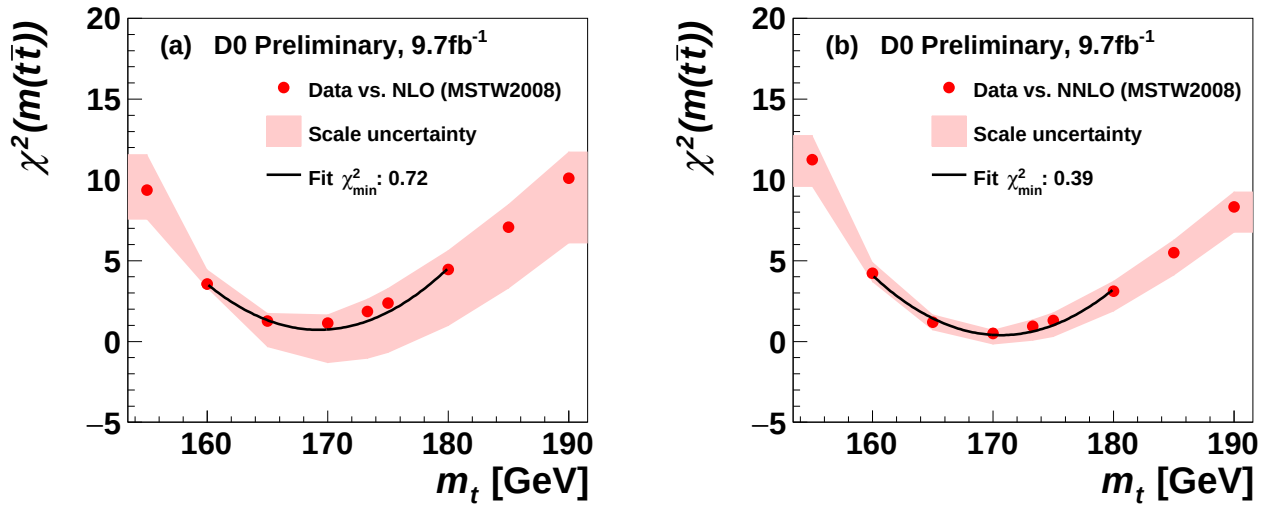

FIG. 5. The χ^2 distribution for the differential cross section as a function of $m(t\bar{t})$ calculated at (a) NLO and (b) at NNLO. The shaded band indicates the theoretical uncertainties while the experimental uncertainties are included in the χ^2 function.

using the differential cross section as a function of $p_T^{\rm top}$ is shown in Fig. 6 at (a) NLO and at (b) NNLO. We combine

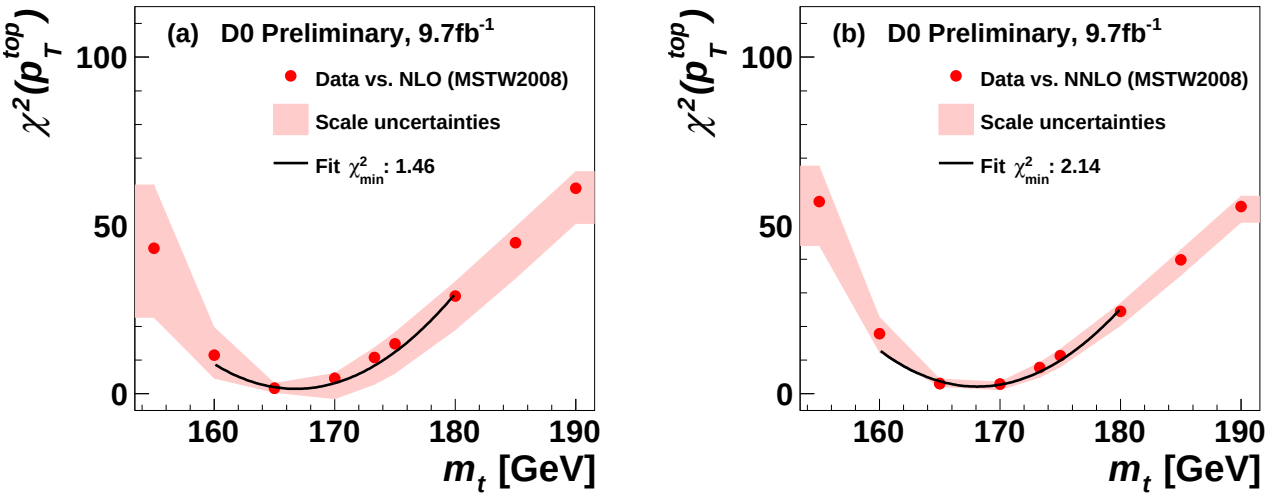

FIG. 6. The χ^2 distribution for the differential cross section as a function of $p_T^{\rm top}$ calculated at (a) NLO and (b) at NNLO. The shaded band indicates the theoretical scale uncertainties.

the $p_T^{\rm top}$ and $m(t\bar{t})$ χ^2 distributions to calculate a combined χ^2, taking into account the correlation between $p_T^{\rm top}$ and $m(t\bar{t})$. A global correlation of 0.12 is determined from the MC@NLO MC showing that the correlation is not large, but for the derivation of the combined χ^2 the entire 2D matrix of $m(t\bar{t})$ vs. $p_T^{\rm top}$ is employed. The combined χ^2 distribution for the differential cross sections as a function of $m(t\bar{t})$ and $p_T^{\rm top}$ is shown in Figure 7(a) at NLO and in (b) at NNLO; the combination is mainly constrained by the $p_T^{\rm top}$ distribution.

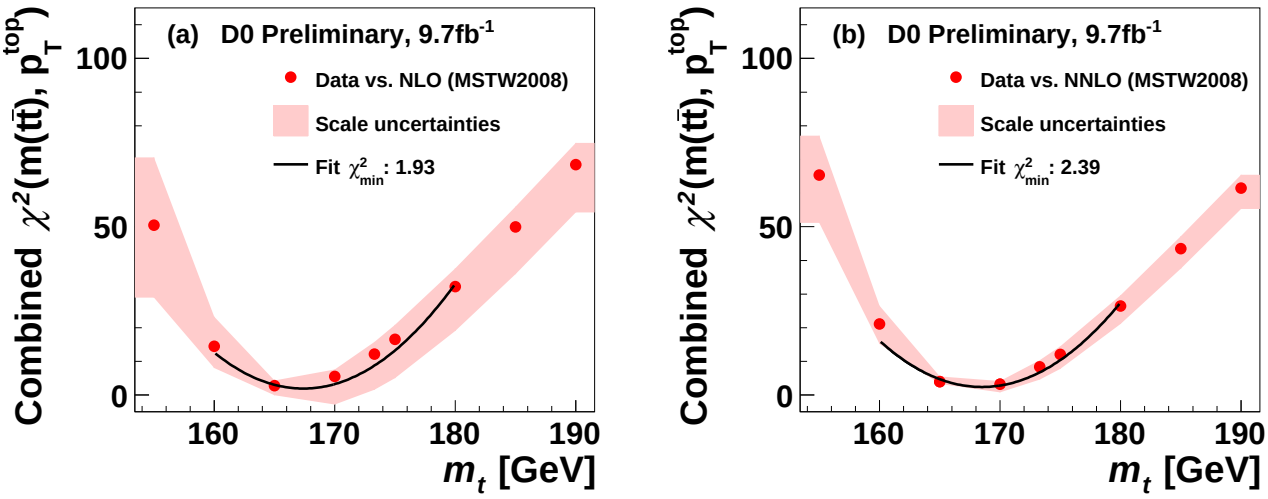

FIG. 7. The combined χ^2 distribution for the differential cross sections in terms of $m(t\bar{t})$ and $p_T^{\rm top}$ calculated at (a) NLO and (b) at NNLO (right). The shaded band indicates the theoretical scale uncertainties.

Order & PDF	$m_t^{\rm pole}$ [GeV] $m(t\bar{t})$	$p_T^{\rm top}$	$m(t\bar{t}) \oplus p_T^{\rm top}$
NLO:			
MSTW2008	169.3 ± 5.7	166.8 ± 2.9	167.4 ± 2.5
CT10	169.4 ± 5.9	167.9 ± 3.0	167.5 ± 2.6
NNPDF2.3	169.0 ± 6.0	166.4 ± 2.9	167.1 ± 2.5
HERAPDF1.5	167.2 ± 6.4	166.0 ± 2.9	165.1 ± 2.7
NNLO:			
MSTW2008	170.7 ± 5.6	168.0 ± 2.5	168.5 ± 2.3
CT10	171.5 ± 5.5	169.4 ± 2.4	169.7 ± 2.2
NNPDF2.3	171.1 ± 5.6	168.5 ± 2.5	169.0 ± 2.3
HERAPDF1.5	172.6 ± 5.6	170.3 ± 2.6	170.2 ± 2.3

TABLE II. Extracted top quark pole mass at NLO and at NNLO pQCD employing the absolute differential cross section as a function of $m(t\bar{t})$ or $p_T^{\rm top}$ and its combination for the MSTW2008, CT10, NNPDF2.3, and HERAPDF1.5 PDF.

We studied the use of differential cross sections normalized by the respective total $\sigma(t\bar{t})$, which provides smaller systematic uncertainties, since e.g. the uncertainty in luminosity cancels. Extracting $m_t^{\rm pole}$ in the same way as described above from the normalized $m(t\bar{t})$ distribution yields improved sensitivity, however using the $p_T^{\rm top}$ distribution yields a degraded sensitivity compared to using the absolute distributions. The central values of $m_t^{\rm pole}$ are similar but the uncertainties are worse, since most of the sensitivity in $p_T^{\rm top}$ originates from the normalization only.

VI. RESULTS AND DISCUSSION

Table III summarizes the results of this analysis at NLO and NNLO for several PDF sets using the combined χ^2 functions from the absolute $m(t\bar{t})$ and $p_T^{\rm top}$ differential cross sections. Employing NNLO pQCD, the pole mass of the top quark is between 168.5 and 170.2 GeV (at NLO it is between 165.1 and 167.5 GeV), depending on the PDF. The breakdown of uncertainties is determined by repeating the $m_t^{\rm pole}$ extraction while setting either the total experimental or theoretical uncertainty to zero. In case of the theoretical uncertainty we add in quadrature the maximum difference

between the extracted $m_t^{\rm pole}$ value using the up, down or nominal scale choice while setting the experimental uncertainties to zero. We also calculate the average $m_t^{\rm pole}$ from the three global PDF sets (MSTW2008, CT10, and NNPDF23) and estimate an additional PDF uncertainty following the PDF4LHC approach [28]. We add in quadrature the maximum difference between the $m_t^{\rm pole}$ average and the extracted $m_t^{\rm pole}$ value for each of the global PDFs as an additional uncertainty for the PDF choice. At NLO the average $m_t^{\rm pole}$ is $167.3 \pm 2.6\,(\text{tot.})$ $[\pm 2.1\,(\text{exp.}) \pm 1.5\,(\text{scale}) \pm 0.2\,(\text{PDF})]$ GeV, whereas at NNLO it is $169.1 \pm 2.5\,(\text{tot.})$ $[\pm 2.2\,(\text{exp.}) \pm 0.8\,(\text{scale}) \pm 1.2\,(\text{PDF})]$ GeV, where the total uncertainty includes the combination of statistical and systematic from the experimental side, and scale uncertainties as well as parton distribution function uncertainties from the theoretical side. When assigning half of the difference between the average $m_t^{\rm pole}$ and the extracted $m_t^{\rm pole}$ value for each of the global PDFs as PDF uncertainty, we get a total uncertainty that is smaller by 0.1 GeV. Averaging all four PDF sets (including HERAPDF1.5) and assigning half of the difference amongst the extracted $m_t^{\rm pole}$ values yields the same total uncertainties (within 0.2 GeV) and a shift in $m_t^{\rm pole}$ of -0.5 GeV at NLO and $+0.3$ GeV at NNLO.
The inclusive $\sigma(t\bar{t})$ corresponding to the measured top quark pole mass average as provided by Top++ without resummation, as an example for the MSTW2008 PDF, is $8.0^{+0.4}_{-0.9}\,(\text{scale})$ pb at NLO and $8.0^{+0.3}_{-0.4}\,(\text{scale})$ pb at NNLO QCD. These values agree, as expected, well with the inclusive $\sigma(t\bar{t})$ measured from the differential distributions in $m(t\bar{t})$, $7.8 \pm 1.0\,(\text{tot.})$ pb, and $p_T^{\rm top}$, $8.0 \pm 1.1\,(\text{tot.})$ pb.

Order & PDF	$m_t^{\rm pole} \pm \delta_{\rm tot.}$ [GeV] $m(t\bar{t}) \oplus p_T^{\rm top}$	$\delta_{\rm exp}$ [GeV] $m(t\bar{t}) \oplus p_T^{\rm top}$	$\delta_{\rm theo}^{\rm scale}$ [GeV] $m(t\bar{t}) \oplus p_T^{\rm top}$
NLO			
MSTW2008	167.4 ± 2.5	± 2.0	± 1.5
CT10	167.5 ± 2.6	± 2.0	± 1.6
NNPDF2.3	167.1 ± 2.5	± 2.0	± 1.5
HERAPDF1.5	165.1 ± 2.7	± 2.3	± 1.5
NNLO			
MSTW2008	168.5 ± 2.3	± 2.2	± 0.7
CT10	169.7 ± 2.2	± 2.0	± 0.9
NNPDF2.3	169.0 ± 2.3	± 2.1	± 0.8
HERAPDF1.5	170.2 ± 2.3	± 2.2	± 0.7

TABLE III. Extracted $m_t^{\rm pole}$ at NLO and at NNLO employing the combined χ^2 in $m(t\bar{t})$ and $p_T^{\rm top}$ distributions for the MSTW2008, CT10, NNPDF2.3, and HERAPDF1.5 PDF. The special setting to separately determine the theoretical uncertainty (for details see text) neglects the correlations between the bins of a measured distribution.

Figure 8(a) summarizes the extractions of the pole mass at different orders of α_s for different PDFs, whereas (b) shows the average $m_t^{\rm pole}$ at NLO and at NNLO relative to other measurements including also the latest Tevatron and world combinations of direct measurements of the top quark mass. There is a consistent average increase between NLO and NNLO of about 1.8 GeV for MSTW2008, CT10 and NNPDF2.3. An increase between NLO and NNLO of 5.4 GeV is found when comparing $m_t^{\rm pole}$ extracted from using HERAPDF1.5. The increase from NLO to NNLO can be understood from the fact that the cross section is about 5% larger at NNLO, which shifts the extracted pole mass towards higher values of $m_t^{\rm pole}$.

The average value of $m_t^{\rm pole}$ extracted from the absolute differential cross sections at NNLO is about 4 GeV less than that extracted from the total cross section [15]. The experimental measurement of the total $\sigma(t\bar{t})$ of $7.3^{+0.6}_{-0.5}\,(\text{tot.})$ pb [15] is about 9% lower than the total $\sigma(t\bar{t})$ measured from the differential cross sections using $m(t\bar{t})$. In the latter case it is $7.8 \pm 1.0\,(\text{tot.})$ pb, while using $p_T^{\rm top}$ it is $8.0 \pm 1.1\,(\text{tot.})$ pb. The differential measurement was not optimized to measure the total cross section, which resulted in larger uncertainties. Taking into account the systematic uncertainties the difference in total $t\bar{t}$ cross section between the inclusive and differential measurements is not significant. Furthermore, part of the difference can be attributed to different theoretical assumptions; the differential cross section calculation has no NNLL resummation, whereas the inclusive cross section calculation performed with Top++ does. This effect is taken into account in the larger scale uncertainties in the differential pole mass extraction[1].

[1] We point out that after the completion of the present analysis, a new fully differential calculation for top pair production at the LHC became available [31]. The calculation of Ref. [31] uses dynamic scales and at NNLO produces total cross-section that is numerically close to the NNLO+NNLL default one from Top++. No calculations with dynamic scales are yet available for the Tevatron.

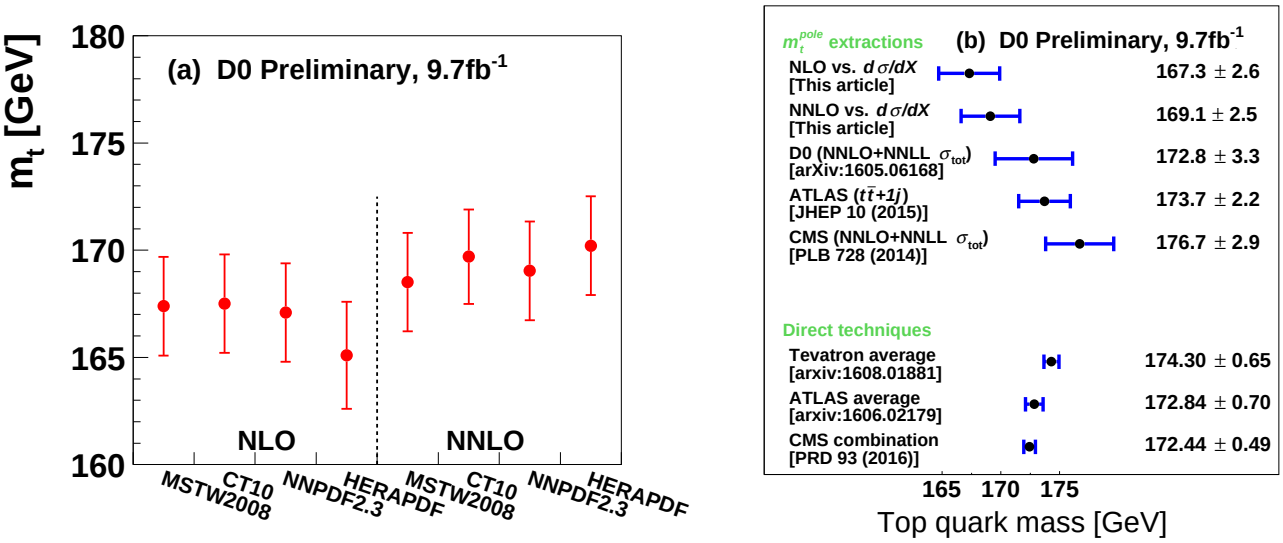

FIG. 8. Extractions of (a) $m_t^{\rm pole}$ at different orders of pQCD and for different PDFs. The average $m_t^{\rm pole}$ is shown in (b) at NLO and at NNLO extracted from the differential cross sections, compared with other $m_t^{\rm pole}$ extractions, as well as with recent direct mass measurements.

VII. CONCLUSIONS

We have made the first measurement of the top quark pole mass based upon the comparison of data with perturbative QCD calculations of the $t\bar{t}$ differential cross sections as a function of $m(t\bar{t})$ and $p_T^{\rm top}$. Comparing to the NLO calculation, we obtain $167.3 \pm 2.6\,(\text{tot.})$ GeV and from comparing to the NNLO calculation we measure $169.1 \pm 2.5\,(\text{tot.})$ GeV. These results are significantly more precise than those based on the total $t\bar{t}$ cross section measurement.

VIII. ACKNOWLEDGMENTS

The work of M.C. was supported in part by grants of the DFG and BMBF. A.M. thanks the Fermilab Theoretical Physics Department for computing support. The work of D.H. and A.M. is supported by the UK Science and Technology Facilities Council [grants ST/L002760/1 and ST/K004883/1]. We thank the staffs at Fermilab and collaborating institutions, and acknowledge support from the Department of Energy and National Science Foundation (United States of America); Alternative Energies and Atomic Energy Commission and National Center for Scientific Research/National Institute of Nuclear and Particle Physics (France); Ministry of Education and Science of the Russian Federation, National Research Center "Kurchatov Institute" of the Russian Federation, and Russian Foundation for Basic Research (Russia); National Council for the Development of Science and Technology and Carlos Chagas Filho Foundation for the Support of Research in the State of Rio de Janeiro (Brazil); Department of Atomic Energy and Department of Science and Technology (India); Administrative Department of Science, Technology and Innovation (Colombia); National Council of Science and Technology (Mexico); National Research Foundation of Korea (Korea); Foundation for Fundamental Research on Matter (The Netherlands); Science and Technology Facilities Council and The Royal Society (United Kingdom); Ministry of Education, Youth and Sports (Czech Republic); Bundesministerium für Bildung und Forschung (Federal Ministry of Education and Research) and Deutsche Forschungsgemeinschaft (German Research Foundation) (Germany); Science Foundation Ireland (Ireland); Swedish Research Council (Sweden); China Academy of Sciences and National Natural Science Foundation of China (China); and Ministry of Education

and Science of Ukraine (Ukraine).

[1] CDF Collaboration, F. Abe *et al.*, Observation of top quark production in $p\bar{p}$ collisions, Phys. Rev. Lett. **74**, 2626 (1995).
[2] D0 Collaboration, S. Abachi *et al.*, Observation of the top quark, Phys. Rev. Lett. **74**, 2632 (1995).
[3] ATLAS Collaboration, G. Aad *et al.*, Observation of a new particle in the search for the Standard Model Higgs boson with the ATLAS detector at the LHC, Phys. Lett. B **716** (2012) 1-29.
[4] CMS Collaboration, S. Chatrchyan *et al.*, Observation of a new boson at a mass of 125 GeV with the CMS experiment at the LHC, Phys. Lett. B **716** (2012) 30.
[5] D0 Collaboration, V. M. Abazov *et al.*, Precision measurement of the top-quark mass in lepton+jets final states, Phys. Rev. Lett. **113**, 032002 (2014).
[6] CMS Collaboration, S. Chatrchyan *et al.*, Measurement of the top quark mass using proton-proton data at $\sqrt{s} = 7$ and 8 TeV , Phys. Rev. D **93** (2016) 072004.
[7] ATLAS, CDF, CMS and D0 Collaborations, First combination of Tevatron and LHC measurements of the top-quark mass only in [arxiv:1403.4427].
[8] CDF & D0 Collaborations, V. M. Abazov *et al.*, Combination of the top-quark mass measurements from the Tevatron collider, Phys. Rev. D **86**, 092003 (2012), updated in [arxiv:1608.01881].
[9] S. Weinzierl, Precision of the top mass, Proceedings of the 50th Rencontres de Moriond on EW Interactions and Unified Theories, (2015).
[10] T. Sjstrand, S. Mrenna and P. Skands, PYTHIA 6.4 Physics and Manual, JHEP05 (2006) 026; A Brief Introduction to PYTHIA 8.1, Comput. Phys. Comm. 178 (2008) 852.
[11] M. Butenschoen, B. Dehnadi, A.H. Hoang, V. Mateu, M. Preisser, I.W. Stewart, Top Quark Mass Calibration for Monte Carlo Event Generators, [arXiv:1608.01318], (2016).
[12] ATLAS Collaboration, G. Aad *et al.*,Determination of the top-quark pole mass using $t\bar{t}$ +1-jet events collected with the ATLAS experiment in 7 TeV pp collisions, JHEP 10 (2015) 121.
[13] CMS Collaboration, S. Chatrchyan *et al.*, Determination of the top-quark pole mass and strong coupling constant from the $t\bar{t}$ production cross section in pp collisions at $\sqrt{s} = 7$ TeV, Phys. Lett. B **728** (2014) 496-517; Corrigendum: Phys. Lett. B **738** (2014) 526-528.
[14] D0 Collaboration, V. M. Abazov *et al.*, Determination of the Pole and $M\bar{S}$ Masses of the Top Quark from the $t\bar{t}$ Cross Section Phys. Lett. B **703**, 422 (2011).
[15] D0 Collaboration, V. M. Abazov *et al.*, Measurement of the inclusive $t\bar{t}$ production cross section in $p\bar{p}$ collisions at $\sqrt{s} = 1.96$ TeV and determination of the top quark pole mass, Subm. to Phys. Rev. D, [arXiv:1605.06168], 2016.
[16] D0 Collaboration, V. M. Abazov *et al.*, Measurement of differential $t\bar{t}$ production cross sections in $p\bar{p}$ collisions Phys. Rev. D **90** 092006 (2014).
[17] M. Czakon, P. Fiedler, D. Heymes and A. Mitov, NNLO QCD predictions for fully-differential top-quark pair production at the Tevatron, JHEP **1605**, 034 (2016).
[18] P. Bärnreuther, M. Czakon and A. Mitov, Percent Level Precision Physics at the Tevatron: First Genuine NNLO QCD Corrections to $q\bar{q} \to t\bar{t} + X$, Phys. Rev. Lett. **109**, 132001 (2012).
[19] M. Czakon and A. Mitov, NNLO corrections to top-pair production at hadron colliders: the all-fermionic scattering channels, JHEP **1212**, 054 (2012).
[20] M. Czakon and A. Mitov, NNLO corrections to top pair production at hadron colliders: the quark-gluon reaction, JHEP **1301**, 080 (2013).
[21] M. Czakon, P. Fiedler and A. Mitov,Total Top-Quark Pair-Production Cross Section at Hadron Colliders Through $O(?\frac{4}{S})$, Phys. Rev. Lett. **110**, 252004 (2013).
[22] M. Czakon and A. Mitov, Top++: A Program for the Calculation of the Top-Pair Cross-Section at Hadron Colliders, Comput. Phys. Commun. **185**, 2930 (2014).
[23] M. Cacciari, M. Czakon, M. Mangano, A. Mitov and P. Nason, Top-pair production at hadron colliders with next-to-next-to-leading logarithmic soft-gluon resummation, Phys. Lett. B **710**, 612 (2012).
[24] A. D. Martin, W. J. Stirling, R. S. Thorne and G. Watt, Parton distributions for the LHC, Eur. Phys. J. C **63**, 189 (2009).
[25] J. Gao *et al.*,CT10 next-to-next-to-leading order global analysis of QCD, Phys. Rev. D **89**, no. 3, 033009 (2014).
[26] R. D. Ball *et al.*, Parton distributions with LHC data, Nucl. Phys. B **867**, 244 (2013).
[27] A. M. Cooper-Sarkar [ZEUS and H1 Collaborations], PDF Fits at HERA, PoS EPS **-HEP2011**, 320 (2011).
[28] J. Butterworth *et al.*. PDF4LHC recommendations for LHC Run II, J. Phys. G: Nucl. Part. Phys. **43** 023001 (2016).
[29] A. Buckley, J. Ferrando, S. Lloyd, K. Nordström, B. Page, M. Rüfenacht, M. Schönherr and G. Watt, LHAPDF6: parton density access in the LHC precision era, Eur. Phys. J. C **75**, 132 (2015).
[30] M. Cacciari, S. Frixione, M. L. Mangano, P. Nason and G. Ridolfi, Updated predictions for the total production cross sections of top and of heavier quark pairs at the Tevatron and at the LHC, JHEP **0809**, 127 (2008).
[31] M. Czakon, D. Heymes, A. Mitov, Dynamical scales for multi-TeV top-pair production at the LHC, [arxiv:1606.03350].
[32] J. Beringer *et al.* (Particle Data Group), Phys. Rev. D **86**, 010001 (2012).
[33] D. L. Phillips, A technique for the numerical solution of certain integral equations of the first kind, J. Assoc. Comp. Mach. **9** (1962) 84–97.

[34] A. N. Tikhonov, On the solution of ill-posed problems and the method of regularization, Soviet Math. Dokl. **4** (1963) 1035 [Dokl. Akad. Nauk. SSSR 151 (1963) 501].
[35] V. Blobel, An unfolding method for high energy physics experiments , Proc. Advanced Statistical Techniques in Particle Physics, Durham (2002).
[36] R. Brun and F. Rademakers, ROOT: An object oriented data analysis framework, Nucl. Instrum. Methods **A389** (1997) 81; S. Schmitt, TUnfold: an algorithm for correcting migration effects in high energy physics, JINST 7 (2012) T10003 [arXiv:1205.6201].
[37] D0 Collaboration, V. M. Abazov *et al.*, Forward-backward asymmetry in top quark-antiquark production, Phys. Rev. D **84**, 112005 (2011).
[38] S. Frixione and B. R. Webber, Matching NLO QCD computations and parton shower simulations, J. High Energy Phys. 06 (2002) 029; S. Frixione *et al.*, J. High Energy Phys. 08 (2003) 007.
[39] G. Corcella, I.G. Knowles, G. Marchesini, S. Moretti, K. Odagiri, P. Richardson, M.H. Seymour, and B.R. Webber, HERWIG 6.5: an event generator for hadron emission reactions with interfering gluons (including supersymmetric processes), J. High Energy Phys. 01 (2001) 010.
[40] M. L. Mangano, M. Moretti, F. Piccinini, R. Pittau, and A.D. Polosa, ALPGEN, a generator for hard multiparton processes in hadronic collisions, J. High Energy Phys. 07 (2003) 001.
[41] T. Sjøstrand, S. Mrenna, and P. Skands, PYTHIA 6.4 physics and manual, J. High Energy Phys. 05 (2006) 026.
[42] D0 Collaboration, V. M. Abazov *et al.*, Precision measurement of the top-quark mass in lepton+jets final states, Phys. Rev. D **91**, 112003.
[43] D0 Collaboration, V. M. Abazov *et al.*, Electron and photon identification in the D0 experiment, Nucl. Instrum. Methods Sect. A **750**, 78 (2014).
[44] D0 Collaboration, V. M. Abazov *et al.*, Muon reconstruction and identification with the Run II D0 detector, Nucl. Instrum. Methods Sect. A **737**, 281 (2014).
[45] D0 Collaboration, V.M. Abazov *et al.*, Jet energy scale determination in the D0 experiment, Nucl. Instrum. Methods in Phys. Res. Sect. A **763**, 0 (2014).
[46] D0 Collaboration, V. M. Abazov *et al.*, Improved b quark jet identification at the D0 experiment, Nucl. Instrum. Methods Sect. A **763**, 290 (2014).